X-ray Absorption and Resonant X-ray Emission at the Carbon Edge of Li_2CO_3

John Vinson,[1, a)] Terrence Jach,[1, b)] Rainer Unterumsberger,[2, c)] Michael A. Woodcox,[1] and Burkhard Beckhoff[2]
[1)] *Material Measurement Laboratory, National Institute of Standards and Technology, Gaithersburg, MD 20899*
[2)] *Physikalisch-Technische Bundesanstalt, Abbestraße 2-12, 10587 Berlin, Germany*

(Dated: 5 August 2026)

While highly successful, density functional theory is known to have limitations owing to its neglect of many-body electron-electron interactions. This neglect leads to errors in the single-particle energies, leading to underestimated band gaps and band widths as well as errors in band alignment at interfaces. Many-body perturbation theory, in the form of the GW self-energy correction, has been widely used to improve upon these short-comings. Though less well studied, the same GW method is also able to predict the finite quasiparticle lifetime that is seen to cause anomalous broadening in the lowest-lying lines of valence emission spectra. Using near-edge x-ray absorption and emission, we probe the electronic structure of Li_2CO_3. Our measurements are compared to first-principles calculations, including GW self-energy corrections to the single-particle energies and excitonic effects from the Bethe-Salpeter equation.

I. INTRODUCTION

Recent work has highlighted the role of valence-band lifetime broadening in x-ray emission spectra, with examples of both nitrates[1–3], and sulfates[4]. It is expected that substantial valence-band broadening will be present in any system with a large splitting between bonding and anti-bonding orbitals, exceeding the band gap of the system. Ionic solids with polyatomic ions often fulfill this criterion. In this work we examine the near-edge x-ray absorption spectra (XAS) and resonant inelastic x-ray scattering (RIXS) spectra at the carbon K edge of Li_2CO_3. X-ray spectroscopy provides a valuable tool for probing the electronic structure of materials and critiquing first-principles simulations. As a probe, x-rays are generally insensitive to surfaces, providing a better match for periodic, bulk-like simulations. The localized nature of the core levels and (for soft x-rays) dipole-limited transitions mean that x-ray absorption and emission probe a subset of the electronic states, focusing the comparison to theoretical calculations.

The carbonate anion is isostructural and isoelectronic with the nitrate anion, previously explored in Refs. 1–3. Previous near-edge x-ray spectroscopy studies of Li_2CO_3 have investigated the oxygen K-edge emission[5], absorption[6], and resonant inelastic x-ray scattering (RIXS)[7]. Measurements and calculations have also been carried out of the Li K edge[8] and non-resonant inelastic scattering at the carbon K edge[9]. In this work we carry out a joint computational and experimental investigation of Li_2CO_3, focusing on x-ray absorption and emission at the carbon K edge. While the previous x-ray emission studies have focused on the upper valence bands, we include the entire valence band. We find a large broadening of emission features from the lower valence bands which are explained by our calculations as resulting from electron-electron scattering, in agreement with previous studies on nitrates[1–3]. A combination of first-principles density-functional theory (DFT) and Bethe-Salpeter equation (BSE) calculations reproduces the major features of the measured spectra.

II. COMPUTATIONAL DETAILS

Our computational investigation of the x-ray spectra is anchored by BSE calculations of both the absorption and resonant emission. The BSE method simplifies the many-body problem, perturbatively considering a single electron-hole excitation on top of the ground state. Typically, the ground state used in BSE calculations is determined at either the DFT level or using many-body corrections to DFT through the GW method. Here we incorporate approximate GW corrections to the single-electron energies of the occupied states, including, crucially, an imaginary component, which corresponds to the (inverse) lifetime of the valence holes. Due to the expense of GW calculations on the dense k-point grids used in the BSE, we applied only band-averaged self-energy corrections. Lastly, we also consider the role of the atomic positions and thermal disorder on the spectra. Our DFT, and hence GW and BSE, is carried out within the Born-Oppenheimer approximation and depends parametrically on the atomic coordinates. Molecular dynamics simulations of a 96-atom supercell were carried out to incorporate thermal disorder, and these structures were used for our BSE simulations of the absorption and emission spectra.

The crystal structure of Li_2CO_3 is monoclinic with the space group C2/c. The ground state of Li_2CO_3 was investigated within DFT using the PBE functional[10]. Calculations were carried out using ABINIT[11,12], and pseudopotentials from Pseudo-Dojo[13,14] generated via

[a)] Electronic mail: john.vinson@nist.gov
[b)] Electronic mail: terrence.jach@nist.gov
[c)] Electronic mail: rainer.unterumsberger@helmut-fischer.com; Present address: Helmut Fischer GmbH Institut für Elektronik und Messtechnik, Industriestraße 21, 71069 Sindelfingen, Germany

TABLE I. Structure of Li_2CO_3 calculated with DFT and compared to previous experimental measurements.

	Neutron[a]	X-ray[b]	DFT
a (Å)	8.35663(10)	8.3593(36)	8.35263
b (Å)	4.97593(6)	4.9725(11)	4.97353
c (Å)	6.19205(7)	6.1975(21)	6.18942
β (°)	114.679(1)	114.83(3)	114.677
V (Å^3)	233.959(3)	233.8	233.640

[a] from Ref. 17.
[b] from Ref. 18.

ONCVPSP[15,16]. The atomic positions and lattice parameters were relaxed to achieve forces with magnitudes less than 1×10^{-5} Ha/Bohr and stresses below 6×10^{-5} Ha/Bohr^3. The resulting cell and atomic positions are in reasonable agreement with experiment (see Table I)[17,18] as well as previous DFT studies[19]. A planewave cutoff energy of 52.6 Ha and k-point sampling of 10^3 were employed.

Partial eigenvalue self-consistent *ev-GW*^{0} corrections were calculated on a 4^3 k-point grid for the lowest 16 conduction band states and all occupied bands. The electron orbitals were held fixed, and the screened Coulomb potential was calculated only with the initial DFT energies. (Note however that while the Li 1*s* states are treated as valence, the parameters for our *GW* corrections are insufficient to give accurate corrections for them.) The dielectric response was calculated with an energy cutoff of 16 Ha and the orbitals were downsampled to this cutoff as well. The response was calculated along the real axis up to 22.8 eV at 0.4 eV spacing and for 10 frequencies along the imaginary axis, using the default exponentially increasing grid. The frequency dependence was determined via the spectral method using 4000 frequency points and the triangular approximation to the delta function[20]. The self-energy corrections were then determined using contour deformation with the orbitals downsampled to an energy cutoff of 30 Ha. For the screening calculation 1024 bands were included while for the self-energy 1052 were used.

Vibrational disorder in Li_2CO_3 was investigated using *ab initio* molecular dynamics (AIMD) within density functional theory. Simulations were performed on a $2 \times 2 \times 2$ supercell (96 atoms) using the Vienna *Ab initio* Simulation Package (VASP)[21–23], using projector-augmented wave (PAW) potentials[24] to treat electron–ion interactions. A plane-wave kinetic energy cutoff of 500 eV was used for these calculations. Exchange–correlation effects were described by the Perdew–Burke–Ernzerhof (PBE) functional[10]. Brillouin zone integrations employed a Γ-centered $5 \times 5 \times 5$ Monkhorst–Pack grid[25] with Gaussian smearing. The computational setup is consistent with our previous work[4].

To generate thermally disordered configurations, the system was gradually heated from 0 K to 298 K at a rate of 1 K/fs within the canonical (NVT) ensemble. A reduced time step of 0.1 fs was employed during this temperature ramp to ensure stable integration of the ionic equations of motion. After reaching 298 K, the time step was increased to 1 fs, and the system was equilibrated for 10 ps at constant temperature. A subsequent production simulation was performed at 298 K. Atomic configurations were extracted at a 2.5 ps interval from 0 ps to 5 ps and 32.5 ps to 37.5 ps, yielding 10 snapshots spanning both the early and late stages of the production trajectory. This sampling strategy provides representative coverage of the full simulation window and verifies sustained equilibration at 298 K.

X-ray calculations were carried out via the Bethe-Salpeter Equation (BSE) method using the OCEAN code, version 3.2.1[26,27]. Wave functions were calculated using QUANTUM ESPRESSO version 7.4[28], using the same functional and pseudopotentials as the *GW* corrections. X-ray absorption spectra are generated by averaging over all 16 carbon sites in the supercell and 3 orthogonal polarization directions. RIXS calculations were averaged over 6 pairs of orthogonal polarizations, mimicking the experimental scattering geometry. For both XAS and RIXS, DFT conduction-band states included approximately 60 eV above the conduction band minimum (1110 empty bands) on a 3^3 k-point mesh, while the core-hole screening was calculated with 2388 empty bands on a 2^3 k-point mesh, encompassing approximately 100 eV above the conduction band minimum. The screening was calculated using an adiabatic time-dependent DFT correction to the vertex[29]. 10 snapshots were taken from the AIMD simulation and x-ray spectra were averaged over them.

RIXS spectra were also calculated using OCEAN, with the same settings as the XAS calculations. Intermediate core-hole excitons were constructed using the generalized minimal residual (GMRES) method[30], while the valence loss function was constructed using Haydock recursion with 100 iterations[31,32]. For all the methods an effective broadening of 0.1 eV was included. A discussion of both methods can be found in Ref. 27. The Li 1*s* orbitals are included within the DFT calculations (an all-electron pseudopotential), but were excluded for the RIXS, corresponding to the lowest 32 bands. The energies of the occupied bands included an approximate, k-point averaged *GW* energy correction, based on the calculation of the unit cell. As discussed later, the only occupied bands with substantial imaginary *GW* components are well-separated in energy, and therefore the broadening correction was carried out as a post-processing step based upon loss energy.

III. EXPERIMENTAL DETAILS

The measurements were carried out on the U49 undulator beamline of the Physikalisch-Technische Bundesanstalt at the electron storage ring BESSY II. The beamline consisted of a plane grating soft x-ray

monochromator and a spherical grating spectrometer configured in the Rowland circle geometry[33,34]. The spectrometer used a grating of 1200 lines/mm on a Rowland circle of 2.5 m radius with a CCD detector[35], and optimal correction formulas for the curvature of the elastic peak on the CCD in this spectrometer are described elsewhere[36]. The spectrometer was oriented in the plane of polarization of the incident beam at a scattering angle of 90° (p-polarization). The monochromator was calibrated in the vicinity of the carbon K edge by the x-ray absorption spectrum through a gas cell as detected by a photodiode. The beam intensity was normalized with the empty gas cell to eliminate the absorption of carbon present on any of the optical surfaces and in the gas cell windows. Calibration was accomplished with CO_2 gas at a pressure of 3 Pa. A linear fit of the energies of the four major absorption peaks of CO_2 gas between 290 eV and 297 eV[37] gave a standard error of 2 meV. The spherical grating spectrometer was then calibrated by quasielastic scattering of the monochromator beam from highly aligned pyrolytic graphite (HAPG), as well as from the Li_2CO_3. The standard error of this calibration between 289 eV and 295 eV, including the uncertainty of the absolute energy scale of the monochromator, was 63 meV. Fits to the width of the quasielastic scattering from HAPG indicated that the resolution of the spectrometer was 0.50 eV, Gaussian full width at half maximum (FWHM).

The sample consisted of Li_2CO_3 powder pressed into indium foil. It was then mounted in ultra-high vacuum at an angle of 45° to both the incident beam and the spectrometer. The x-ray absorption spectrum was recorded by C Kα fluorescence from the sample using a silicon drift detector. The mass absorption coefficient due to non-resonant energy levels was less than 3% of the resonant absorption, so no self-absorption correction was applied. Emission spectra were recorded at a series of excitation energies above the C K-edge designated in Fig. 3. Each spectrum represents 7200 s of counting time except for 5400 s during the final spectrum at 321.7 eV.

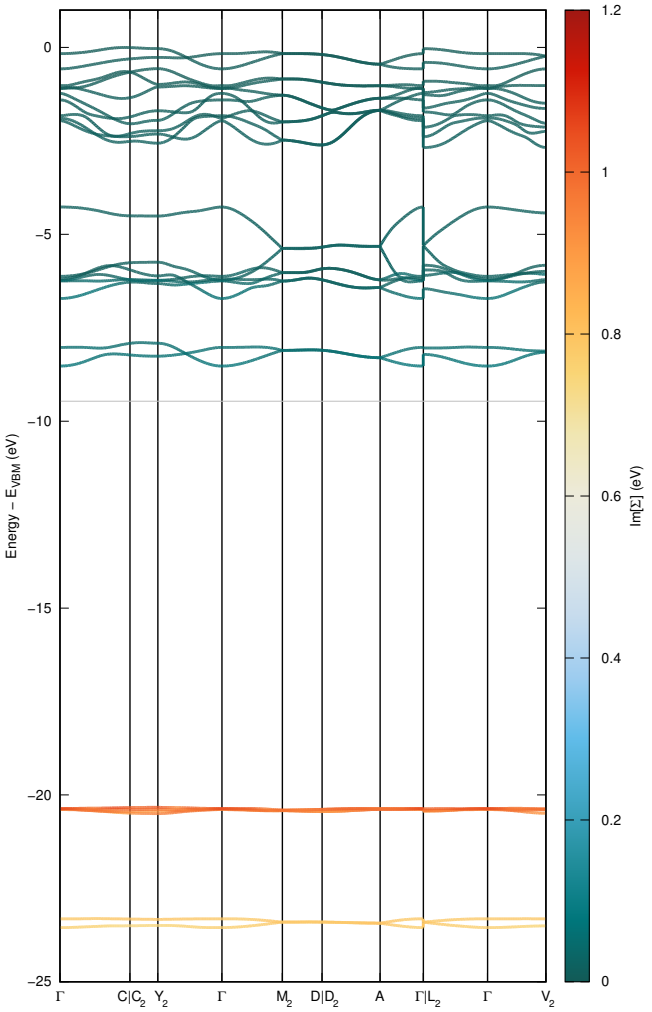

FIG. 1. Band structure of Li_2CO_3 determined from DFT calculations with G^0W^0 corrections, where 0 is the top of the valence bands (located at C). The bands are colored based on the complex value of their GW correction. The grey line at −9.47 eV is the energy below the top of the valence band corresponding to the value of the calculated GW band gap. The conduction band is not shown, but its minimum is at Γ.

IV. RESULTS

A. Electronic Structure

The GW-corrected band structure of the occupied bands is shown in Fig. 1. The conduction band minimum (not shown) is at Γ, with a calculated band gap of 9.47 eV compared to a DFT gap of 5.14 eV. The bands are color-coded by the magnitude of the imaginary component of the GW correction, which is inversely proportional to the quasiparticle lifetime. As has been shown in other materials[1–4], the upper valence bands have very small lifetime broadening. As discussed previously[4], it is only when valence band states are deeper than the band gap below the valence band maximum (VBM) that they are energetically allowed to decay through electron-electron scattering. The entirety of the upper valence bands are within 9 eV of the VBM, and, as expected, the GW calculations indicate that they have little lifetime broadening.

Substantial broadening is associated with the bands near −20 eV and −24 eV. From the projected density of states (pDOS) shown in Fig. 2 we can identify these as the C-O bonding orbitals. In particular, the states near −20 eV have a strong p-like character around the carbon atoms, implying that they should have a strong transition in x-ray emission spectra (XES) at the carbon K edge. From both the band structure and density of states plots, we can see that these states have very little dispersion. In the absence of self-energy broadening, emission peaks associated with them would be expected to be quite sharp. As a point of reference, the carbon

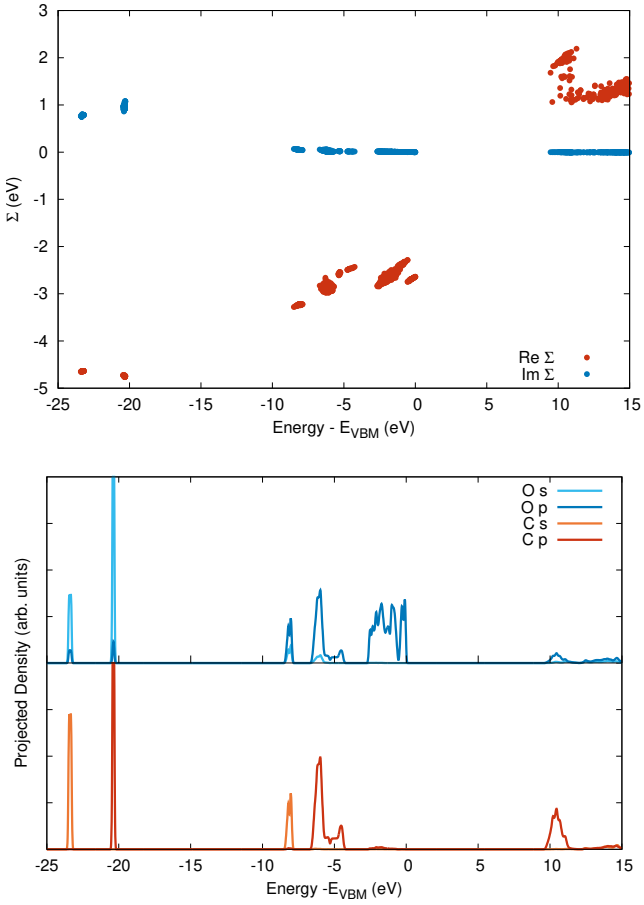

FIG. 2. Top) the GW corrections as a function of the GW-corrected energies, relative to the valence band maximum (VBM). Bottom) Projected density of states (pDOS) of Li_2CO_3 determined from DFT calculations with G^0W^0 corrections, relative to the valence band maximum.

1s lifetime broadening is taken to be 0.1 eV, which corresponds to a lifetime around 10 times longer than these lower valence bands. We also see that the conduction band minimum has a strong carbon p component, while the upper valence bands are nearly entirely associated with anti-bonding states around the oxygen atoms. A comparison of the relative spacing of the valence bands to photoemission spectra of Li_2CO_3 indicates that our GW calculations may have overestimated the binding of these deep valence states[38], which is corroborated by our x-ray emission comparison in Sec. IV C.

B. X-ray Absorption

In polyatomic or molecular ions, the local electronic environment around the central atom is less sensitive to the specific counterion as the strong intramolecular bonds dominate over the weaker ionic ones. This is born out in the strong family resemblance in near-edge x-ray absorption measurements of the central element. In

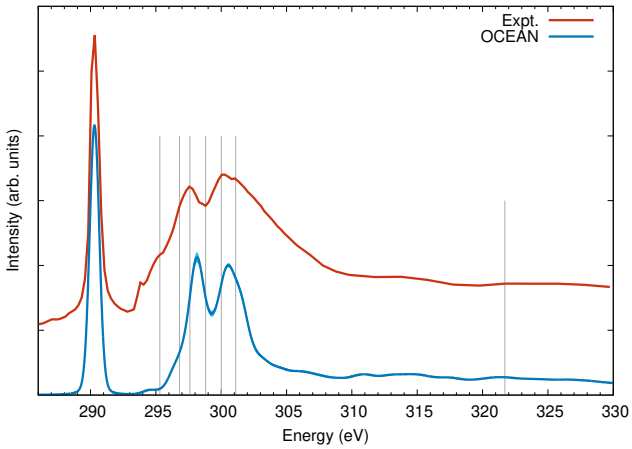

FIG. 3. X-ray absorption at the carbon K edge. The theory is aligned to match the strong peak at 290 eV, and the two spectra are offset vertically for clarity. Lighter blue shading denotes the variance of the calculated average spectra, which is smaller than the line thickness except near 298 eV (see discussion in Appx. A). Vertical lines show the incident energies the correspond to the RIXS spectra in Fig. 4 (five, closely spaced spectra taken near 290 eV are not marked).

Fig. 3 we see the main features of the carbon K edge, a strong, narrow, and well-separated π^* exciton followed by a much broader σ^* peak or set of peaks that is common to carbonates[39,40].

The strong, well separated π^* exciton at 290 eV is due to excitations into p_z-like states on the carbon, perpendicular to the carbonate plane. Due to its positioning into the empty space above and below the carbonate, this peak is nearly unaffected by thermal disorder. All 10 AIMD snapshots as well as the unit cell give a nearly identical π^* peak, as can be seen in Fig. 5. The exciton is hybridized with p_z states on the neighboring oxygen atoms. To demonstrate this, the photo-electron density of this exciton is plotted in Fig. 6.

The higher-energy, σ^* peaks range from around 296 eV to 302 eV. These excitations are in the CO_3^{2-} plane, involving p_{xy} states on the central carbon and neighboring oxygen atoms, see Fig. 6. Unlike the π^* exciton, the excited-electron density is along the C-O bonds, and therefore, as seen in Fig. 5, these states are sensitive to thermal disorder. However, this sensitivity is mild and, importantly symmetric and peak-independent (excluding the π^* exciton). This means that the thermal disorder is not mixing in dipole-forbidden electronic states. Given the elements and electron filling in CO_3^{2-}, there are no such local, unoccupied states to mix in. This is in contrast to systems such as LiF[8] or Al_2O_3[41] where so-called "dark" (s-like) excitons become dipole allowed due to thermal disorder, or the case of ammonium nitrate, where the broadening is strongly peak dependent[1].

C. Resonant Inelastic X-ray Scattering

Measured and calculated RIXS spectra are shown in Fig. 4. The main features and intensities of the x-ray emission are well-captured by the calculation, especially towards the non-interacting limit. X-ray emission at the carbon K edge is dipole limited, and the emission lines must have some p-type character around the carbon atoms. The states will be in energy ranges that correspond to the pDOS shown in Fig. 2, though the matrix elements, and therefore intensities, can be quite different. Small shifts in emission energy are possible due to the excitonic binding of the final state conduction-electron–valence-hole exciton. This effect is most pronounced near the edge and for spatially small excitons.

The most-bound valence holes created by the x-ray emission process, calculated to be around 20 eV below the valence band maximum, correspond to an x-ray emission energy of around 265 eV. These states can be assigned as $1e'$, with sufficient C $2p_{xy}$ hybridization to be visible. As can be seen in Figs. 1 and 2, these states have almost no dispersion. The observed width is due primarily to the large lifetime broadening from electron-electron scattering or decay, as shown by the self-energy calculations. The strongest emission line (near 279 eV) is made up of CO π- and σ-bonding orbitals. The highest energy emission feature near 283 eV comes from states primarily on the oxygen with weak hybridization with the C p_{xy}.

It is evident that the peak near 265 eV is broader in the measured data than in the experiment, and that it narrows slightly at threshold, incident energy ≈290 eV. From this, we attribute some of the additional observed broadening to dynamic effects, phonon relaxation or scattering, that are neglected in our approach. For excitations on the first exciton, dynamical phonon effects may be suppressed slightly by the compact exciton screening the core hole. The position of this peak in the calculations is too low in energy by approximately 1 eV. This highlights a limitation in our GW calculations, which may arise from starting-point dependence or other shortcomings from incomplete self-consistency. In particular, the differences in localization between the lower valence and upper valence bands may lead to different errors in the shape of the orbitals from the semi-local exchange correlation approximation which are uncorrected by our GW approximation. Previous work using fully eigenvalue-self-consistent GW calculations has also noted a relative overestimation of the binding of the lower valence bands[42], though in that previous work W was recomputed with updated eigenvalues while here we kept W^0. Higher-order methods remain infeasible for condensed systems, but the molecular nature of the carbonate ion might be amenable to cluster approaches with lower scaling costs.

Focusing now on incident energies near 290 eV (bottom of Fig. 4), we see a large emission energy shift in the OCEAN calculations that is only partially present in the measured data. Two separate effects are responsible for the shift in the main emission feature. The measured

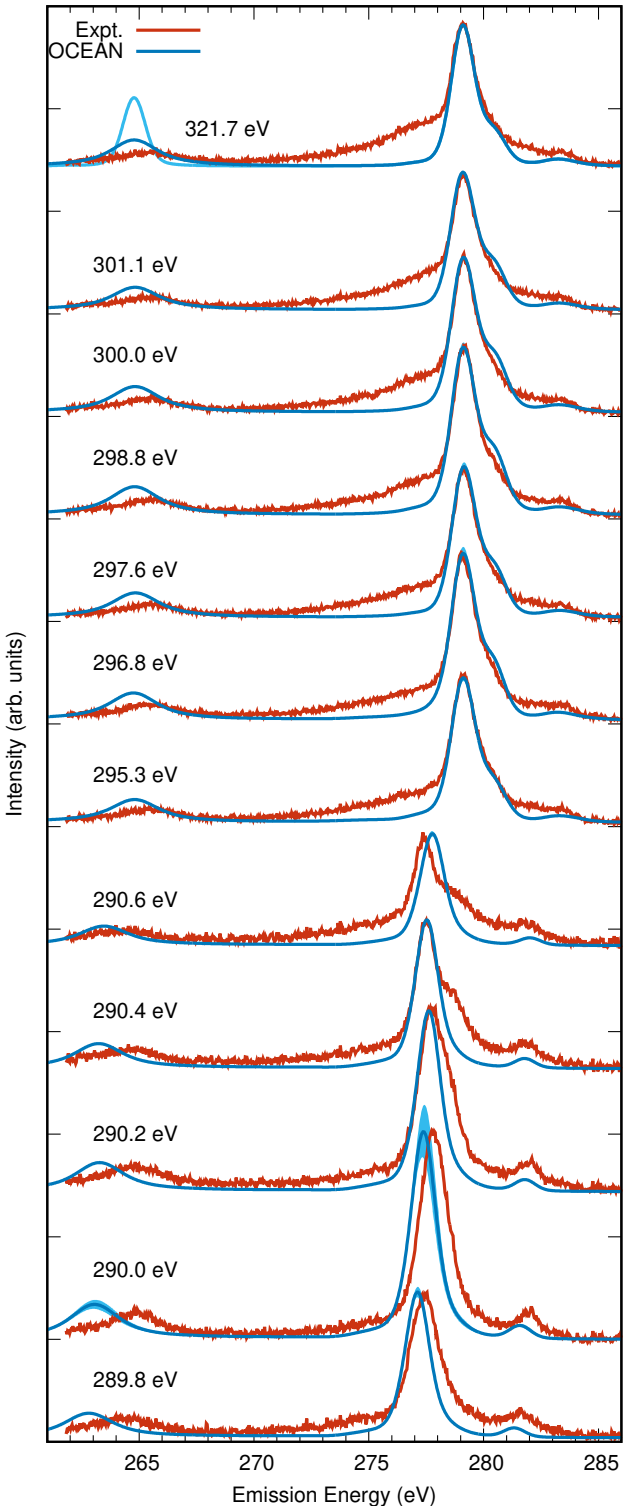

FIG. 4. X-ray emission spectra at various incident x-ray energies. Spectra are offset vertically for clarity, and scaled independently with calculations set to match the main peak height. Again, lighter blue shading indicates the 95% confidence interval based on only 10 MD snapshots, which is only notable at 290.0 eV incident x-ray energy. For an incident energy of 321.7 eV we include the calculation without valence-band lifetime broadening (light blue).

spectra show a shift from 279 eV to 277 eV as the incident energy is reduced from high above the edge down towards threshold. The shift appears binary, with an onset that corresponds with initial excitations into the first exciton. This nearly 2 eV shift is due to excitonic binding in the final state – valence hole and conduction electron. The incompletely filled $2p$ shell results in a highly localized excited electron, while the molecular nature of the system ensures an equally compact hole state. This strong localization results in substantially increased excitonic binding, shifting the emission lines. This effect was previously observed and calculated in the RIXS spectra of lithium peroxide[7], and it should be a general consequence of the strongly localized exciton enabled by a partially filled shell. For an incident x-ray energy of 290.4 eV, it can be seen that the OCEAN calculation adequately captures the shift due to enhanced exciton binding.

Continuing down in energy, the theory and measurement diverge slightly. This is due to a Raman shift in the calculation, indicating that the x-ray absorption excitations are into virtual states with an energy deficit that must be balanced by an emission shift. This may be indicative of too little ground-state vibrational disorder, possibly due to only including thermal disorder in our MD. More likely, the neglect of dynamic phonon scattering is responsible for the observed shift in the calculation, with vibrational coupling making up for the energy losses in the physical system. Indeed phonon scattering could reduce the effect of the Raman shift on either side of the π^* exciton, accounting for the misalignment both above at 290.6 eV and below at 289.8 eV and 290.0 eV.

Lastly, the measured x-ray emission shows spectral weight below the strong emission peak of 279 eV that is unaccounted for in the calculations. This takes the form of an almost linear slope starting near 271 eV, and it is more prominent at higher incident photon energies. We do not believe this to be due to unaccounted-for many-body satellite (plasmon) excitations as those must necessarily be separated from the main peak by more than the band gap (> 9 eV), e.g., starting below 270 eV. At the same time this spectral weight would not be coming from neglected phonon excitations as the energy is much too large. While its origin is not known, the most likely cause of this artifact is emission from graphitic carbon, which has the correct shape and energy range[43].

V. CONCLUSIONS

We have measured and calculated the x-ray absorption and resonant emission at the carbon K edge in Li_2CO_3. As in earlier studies of the nitrogen spectra in nitrates, we have found that emission features from the lower valence band have extreme broadening. We have demonstrated that the majority of this effect is accounted for by electron-electron scattering within the GW approximation. The calculated and observed lifetimes of these states is more than 10 times shorter than that of the $1s$ core hole. Including the complex-valued GW energy correction in the BSE calculations gives good overall agreement between the calculated and measured spectra.

The discrepancies between predicted and observed spectra point to the utility of near-edge x-ray spectroscopy as a benchmark for electronic stucture theory methods. In the non-resonant limit, relative spacing between the main emission peaks, at 265 eV and 279 eV, and the width of the lower-energy peak are both tied directly to the dressed one-electron Green's function and the success of the GW approximation to the electron self-energy. In our calculations, the spacing of the emission features is overestimated by approximately 1 eV. The calculated band gap also appears to be overestimated by approximately 0.5 eV, though the relative alignment between x-ray absorption and emission calculations necessarily involves the stength of the electron-hole interactions which may introduce error. Finally, the broadening of the lowest-energy emission feature is underestimated in the calculations. This is most likely due to only including electron-electron scattering and neglecting excited-state phonon dynamics. This emission peak corresponds to a final-state hole in the CO bonds, making phonon broadening likely, but capturing the vibrational dynamics is beyond the scope of this work.

The data that support the findings of this study are openly available in the NIST Public Data Repository at https://doi.org/10.18434/mds2-4167.

Certain software is identified in this paper in order to specify the experimental procedure adequately. Such identification is not intended to imply recommendation or endorsement of any product or service by NIST, nor is it intended to imply that the software identified is necessarily the best available for the purpose.

[1] J. Vinson, T. Jach, W. T. Elam, and J. D. Denlinger, "Origins of extreme broadening mechanisms in near-edge x-ray spectra of nitrogen compounds," Phys. Rev. B **90**, 205207 (2014).

[2] J. Vinson, T. Jach, M. Müller, R. Unterumsberger, and B. Beckhoff, "Quasiparticle lifetime broadening in resonant x-ray scattering of nh_4no_3," Phys. Rev. B **94**, 035163 (2016).

[3] J. Vinson, T. Jach, M. Müller, R. Unterumsberger, and B. Beckhoff, "Resonant x-ray emission and valence-band lifetime broadening in $lino_3$," Phys. Rev. B **100**, 085143 (2019).

[4] T. Jach, J. Vinson, M. Woodcox, A. Jonas, K. Frenzel, R. Unterumsberger, and B. Beckhoff, "Universality of extreme-broadening mechanisms in some near-edge x-ray spectra," Phys. Rev. B **111**, 125107 (2025).

[5] A. Léon, A. Fiedler, M. Blum, A. Benkert, F. Meyer, W. Yang, M. Bär, F. Scheiba, H. Ehrenberg, L. Weinhardt, and C. Heske, "Valence electronic structure of li2o2, li2o, li2co3, and lioh probed by soft x-ray emission spectroscopy," The Journal of Physical Chemistry C **121**, 5460–5466 (2017).

[6] R. Qiao, Y.-D. Chuang, S. Yan, and W. Yang, "Soft x-ray irradiation effects of li2o2, li2co3 and li2o revealed by absorption spectroscopy," PLOS ONE **7**, 1–6 (2012).

[7] Z. Zhuo, C. D. Pemmaraju, J. Vinson, C. Jia, B. Moritz, I. Lee, S. Sallies, Q. Li, J. Wu, K. Dai, Y.-d. Chuang, Z. Hussain, F. Pan, T. P. Devereaux, and W. Yang, "Spectroscopic signature of oxidized oxygen states in peroxides," The Journal of Physical Chemistry Letters **9**, 6378–6384 (2018).

[8] T. A. Pascal, U. Boesenberg, R. Kostecki, T. J. Richardson, T.-C. Weng, D. Sokaras, D. Nordlund, E. McDermott, A. Moewes, J. Cabana, and D. Prendergast, "Finite temperature effects on the x-ray absorption spectra of lithium compounds: First-principles interpretation of x-ray raman measurements," The Journal of Chemical Physics **140**, 034107 (2014).

[9] E. de Clermont Gallerande, D. Cabaret, G. Lelong, C. Brouder, M.-B. Attaiaa, L. Paulatto, K. Gilmore, C. J. Sahle, and G. Radtke, "First-principles modeling of x-ray raman scattering spectra," Phys. Rev. B **98**, 214104 (2018).

[10] J. P. Perdew, K. Burke, and M. Ernzerhof, "Generalized gradient approximation made simple," Phys. Rev. Lett. **77**, 3865–3868 (1996).

[11] `www.abinit.org` *v.* 10.0.7.

[12] X. Gonze, F. Jollet, F. A. Araujo, D. Adams, B. Amadon, T. Applencourt, C. Audouze, J.-M. Beuken, J. Bieder, A. Bokhanchuk, E. Bousquet, F. Bruneval, D. Caliste, M. Cote, F. Dahm, F. D. Pieve, M. Delaveau, M. D. Gennar, B. Dorado, C. Espejo, G. Geneste, L. Genovese, A. Gerossier, M. Giantomassi, Y. Gillet, D. R. Hamann, L. He, G. Jomard, J. L. Janssen, S. L. Roux, A. Levitt, A. Lherbier, F. Liu, I. Lukacevic, A. Martin, C. Martins, M. J. T. Oliveira, S. Ponce, Y. Pouillon, T. Rangel, G.-M. Rignanese, A. H. Romero, B. Rousseau, O. Rubel, A. A. Shukri, M. Stankovski, M.Torrent, M. J. V. Setten, B. V. Troeye, M. J. Verstraete, D. Waroquier, J. Wiktor, B. Xue, A. Zhou, and J. W. Zwanziger, "Recent developments in the ABINIT software package," Comput. Phys. Comm. **205**, 106 (2016).

[13] `http://www.pseudo-dojo.org` Scalar-relativstic *v.* 0.4.

[14] M. J. van Setten, M. Giantomassi, E. Bousquet, M. J. Verstraete, D. R. Hamann, X. Gonze, and G.-M. Rignanese, "The pseudodojo: Training and grading a 85 element optimized norm-conserving pseudopotential table," Comput. Phys. Commun. **226**, 39–54 (2018).

[15] The open-source code ONCVPSP is available at `http://www.mat-simresearch.com` *v.* 3.3.1.

[16] D. R. Hamann, "Optimized norm-conserving vanderbilt pseudopotentials," Phys. Rev. B **88**, 085117 (2013).

[17] Y. Idemoto, J. W. Richardson, N. Koura, S. Kohara, and C.-K. Loong, "Crystal structure of (lixk1 - x)2co3 (x = 0, 0.43, 0.5, 0.62, 1) by neutron powder diffraction analysis," Journal of Physics and Chemistry of Solids **59**, 363–376 (1998).

[18] H. Effenberger and J. Zemann, "Verfeinerung der kristallstruktur des lithiumkarbonates, li_2co_3," Z. Kristallogr. **150**, 133–138 (1979).

[19] Y. Duan and D. C. Sorescu, "Density functional theory studies of the structural, electronic, and phonon properties of li_2O and li_2co_3: Application to co_2 capture reaction," Phys. Rev. B **79**, 014301 (2009).

[20] M. Shishkin and G. Kresse, "Implementation and performance of the frequency-dependent *gw* method within the paw framework," Phys. Rev. B **74**, 035101 (2006).

[21] G. Kresse and J. Hafner, "Ab initio molecular dynamcis for liquid metals," Phys. Rev. B **47**, 558 (1993).

[22] J. Furthmüller and G. Kresse, "Efficiency of ab-initio total energy calculations for metals and semiconductors using a plane-wave basis set," Comput. Mater. Sci. **6**, 15–50 (1996).

[23] G. Kresse and J. Furthmüller, "Efficient iterative schemes for ab initio total-energy calculations using a plane-wave basis set," Phys. Rev. B **54**, 11169–11186 (1996).

[24] P. E. Blöchl, "Projector augmented-wave method," Phys. Rev. B **50**, 17953–17979 (1994).

[25] H. J. Monkhorst and J. D. Pack, "Special points for brillouin-zone integrations," Physical Review B **13**, 5188–5192 (1976).

[26] J. Vinson, J. J. Rehr, J. J. Kas, and E. L. Shirley, "Bethe-salpeter equation calculations of core excitation spectra," Phys. Rev. B **83**, 115106 (2011).

[27] J. Vinson, "Advances in the ocean-3 spectroscopy package," Phys. Chem. Chem. Phys. **24**, 12787–12803 (2022).

[28] P. Giannozzi, O. Andreussi, T. Brumme, O. Bunau, M. Buongiorno Nardelli, M. Calandra, R. Car, C. Cavazzoni, D. Ceresoli, M. Cococcioni, N. Colonna, I. Carnimeo, A. Dal Corso, S. de Gironcoli, P. Delugas, R. A. DiStasio, A. Ferretti, A. Floris, G. Fratesi, G. Fugallo, R. Gebauer, U. Gerstmann, F. Giustino, T. Gorni, J. Jia, M. Kawamura, H.-Y. Ko, A. Kokalj, E. Küçükbenli, M. Lazzeri, M. Marsili, N. Marzari, F. Mauri, N. L. Nguyen, H.-V. Nguyen, A. Otero-de-la Roza, L. Paulatto, S. Poncé, D. Rocca, R. Sabatini, B. Santra, M. Schlipf, A. P. Seitsonen, A. Smogunov, I. Timrov, T. Thonhauser, P. Umari, N. Vast, X. Wu, and S. Baroni, "Advanced capabilities for materials modelling with quantum espresso," Journal of Physics: Condensed Matter **29**, 465901 (2017).

[29] J. Vinson and E. L. Shirley, "Fast, efficient, and accurate dielectric screening using a local real-space approach," Phys. Rev. B **103**, 245143 (2021).

[30] Y. Saad and M. H. Schultz, "Gmres: A generalized minimal residual algorithm for solving nonsymmetric linear systems," SIAM Journal on Scientific and Statistical Computing **7**, 856–869 (1986).

[31] R. Haydock, "The recursive solution of the schrödinger equation," Computer Physics Communications **20**, 11–16 (1980).

[32] L. X. Benedict and E. L. Shirley, "Ab initio calculation of $\epsilon_2(\omega)$ including the electron-hole interaction: Application to gan and caf_2," Phys. Rev. B **59**, 5441–5451 (1999).

[33] F. Senf, U. Flechsig, F. Eggenstein, W. Gudat, R. Klein, H. Rabus, and G. Ulm, "A plane-grating monochromator beamline for the ptb undulators at bessy ii," J. Synchrotron Radiat. **5**, 780–782 (1998).

[34] F. Scholze, B. Beckhoff, G. Brandt, R. Fliegauf, R. Klein, B. Meyer, D. Rost, D. Schmitz, M. Veldkamp, J. Weser, G. Ulm, E. Louis, A. E. Yakshin, S. Oestreich, and F. Bijkerk, "New ptb beamlines for high-accuracy euv reflectometry at bessy ii," Proc. SPIE **4146**, 72 (2000).

[35] R. Unterumsberger, M. Müller, B. Beckhoff, P. Hönicke, B. Pollakowski, and S. Bjeoumikhova, "Focusing of soft x-ray radiation and characterization of the beam profile enabling x-ray emission spectrometry at nanolayered specimens," Spectrochimica Acta Part B: Atomic Spectroscopy **78**, 37 (2012).

[36] M. Müller, B. Beckhoff, R. Fliegauf, and B. Kanngießer, "Nickel L_{iii} fluorescence and satellite transition probabilities determined with an alternative methodology for soft-x-ray emission spectrometry," Phys. Rev. A **79**, 032503 (2009).

[37] G. Wight and C. E. Brion, "K-shell energy loss spectra of 2.5 kev electrons in CO_2 and N_2O," J. Electron. Spectrosc. Relat. Phenom. **3**, 191 (1974).

[38] R. Dedryvère, L. Gireaud, S. Grugeon, S. Laruelle, J.-M. Tarascon, and D. Gonbeau, "Characterization of lithium alkyl carbonates by x-ray photoelectron spectroscopy: Experimental and theoretical study," The Journal of Physical Chemistry B **109**, 15868–15875 (2005).

[39] J. A. Brandes, S. Wirick, and C. Jacobsen, "Carbon *K*-edge spectra of carbonate minerals," Journal of Synchrotron Radiation **17**, 676–682 (2010).

[40] D. Zhou, R. A. Metzler, T. Tyliszczak, J. Guo, M. Abrecht, S. N. Coppersmith, and P. U. P. A. Gilbert, "Assignment of polarization-dependent peaks in carbon k-edge spectra from biogenic and geologic aragonite," The Journal of Physical Chemistry B **112**, 13128–13135 (2008), pMID: 18811192.

[41] C. Brouder, D. Cabaret, A. Juhin, and P. Sainctavit, "Effect of atomic vibrations on the x-ray absorption spectra at the k edge of al in α-al_2o_3 and of ti in tio_2 rutile," Phys. Rev. B **81**, 115125 (2010).

[42] N. Marom, F. Caruso, X. Ren, O. T. Hofmann, T. Körzdörfer, J. R. Chelikowsky, A. Rubio, M. Scheffler, and P. Rinke, "Benchmark of *gw* methods for azabenzenes," Phys. Rev. B **86**, 245127 (2012).

[43] J. A. Carlisle, E. L. Shirley, L. J. Terminello, J. J. Jia, T. A. Callcott, D. L. Ederer, R. C. C. Perera, and F. J. Himpsel, "Band-structure and core-hole effects in resonant inelastic soft-x-ray scattering: Experiment and theory," Phys. Rev. B **59**, 7433–7445 (1999).

[44]K. Momma and F. Izumi, "*VESTA*: a three-dimensional visualization system for electronic and structural analysis," Journal of Applied Crystallography **41**, 653–658 (2008).

Appendix A: Thermal Disorder

In order to capture the effect of disorder, simulations must be carried out on a large enough structure such that the size of the cell does not artificially bias the resulting spectra. X-ray absorption is a local probe, and we chose a 96-atom supercell (16 carbon sites) as a balance between computational cost and systematic error. Next, an average over different snapshots is necessary to converge the results. To indicate the convergence with respect to the number of snapshots, the variance of the mean is determined for the calculated x-ray spectra

$$v^2(\omega) = [N(N-1)]^{-1} \sum_i^N \left(\sigma_i(\omega) - \bar{\sigma}(\omega)\right)^2 \qquad \text{(A1)}$$

where $\bar{\sigma} \pm 2.26v$ gives the approximate 95% confidence interval for the mean spectrum in the infinite-snapshot limit, given our use of 10 snapshots. This confidence interval is indicated as a shaded region in the plots of XAS and RIXS spectra. The scatter in XAS among the 10 AIMD snapshots is shown in Fig. 5. The effect of the thermal disorder is largely captured by Gaussian broadening, though in Fig. 5 it can be seen that the 301 eV peak is broadened slightly more by thermal disorder than the 298 eV peak.

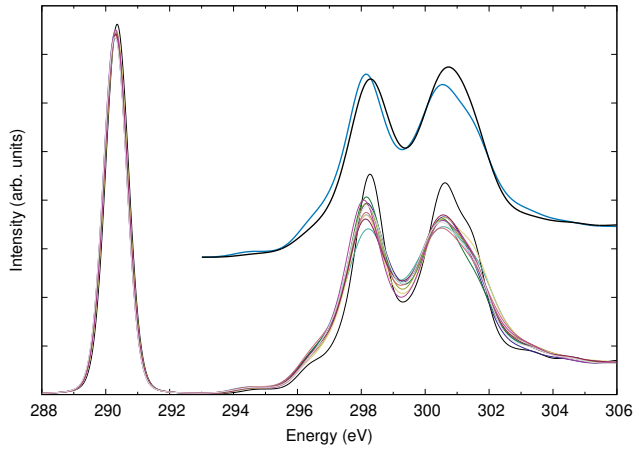

FIG. 5. Calculations of the x-ray absorption at the carbon K edge, showing the differences between the thermal snapshots. The black line is the undistorted unit cell, while the 10 lines of various colors are the 10 AIMD snapshots. All calculations are broadened by the same 0.1 eV core-hole lifetime and an additional 0.8 eV full-width at half-maximum Gaussian. Offset vertically, the average of the 10 snapshots in blue compared to the unit cell broadened further with a 1.2 eV full-width at half-maximum Gaussian.

Appendix B: Exciton densities

Exciton photo-electron densities were calculated for the unit cell at select x-ray absorption energies and polarizations. This procedure is outlined in Ref. 27 and summarized briefly here. The exciton is not treated as an eigenstate of the BSE, but instead it is a sum over eigenstates as selected by the x-ray energy ω and polarization ε.

$$|x_\varepsilon(\omega)\rangle = \frac{1}{\omega - H_{\mathrm{BSE}} + i\Gamma} \hat{d}_\varepsilon |0\rangle \quad , \qquad \text{(B1)}$$

where $|0\rangle$ is the ground state, Γ is the core-hole lifetime, $\hat{d}_\varepsilon$ is the electron-photon operator, and H_{BSE} is the BSE Hamiltonian for the x-ray excitation. The x-ray absorption can be written in terms of x instead of an explicit sum over final states

$$\sigma(\omega;\varepsilon) \propto \langle 0 | d_\varepsilon^\dagger | x_\varepsilon(\omega) \rangle \quad . \qquad \text{(B2)}$$

Summing over the electron and hole states, the exciton photoelectron density can be plotted in real-space as is done in Fig. 6 for three selected energies and polarizations.

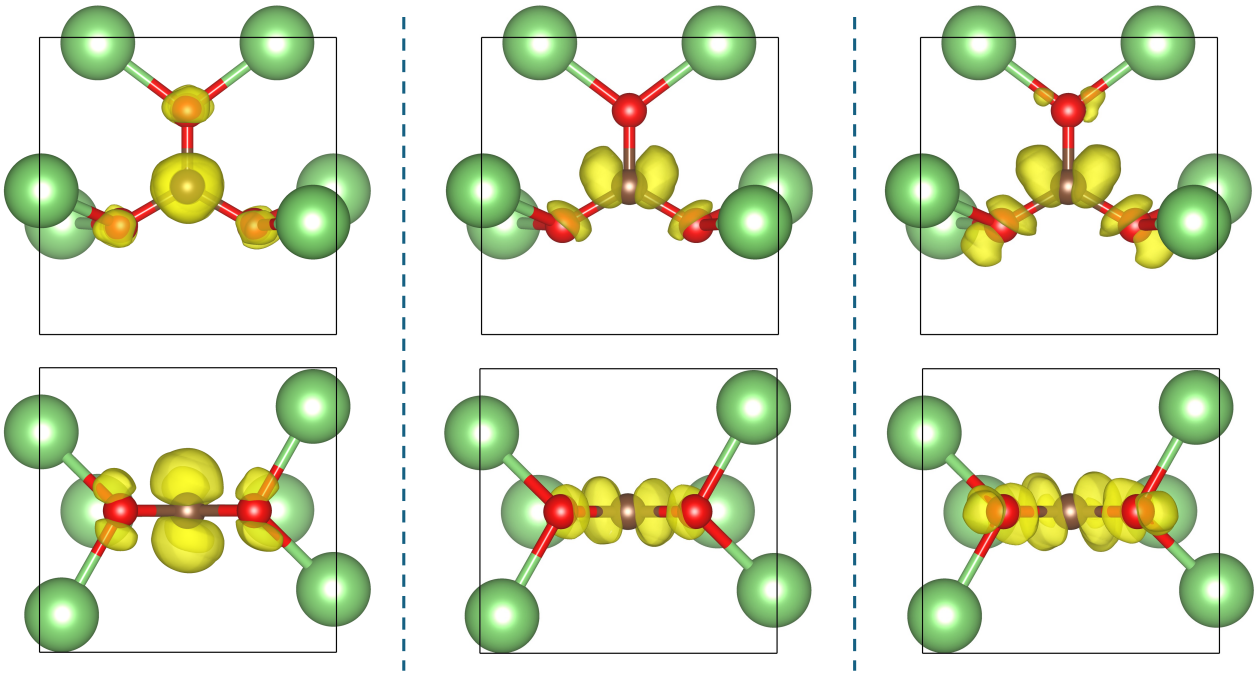

FIG. 6. Calculations of the x-ray absorption photo-electron density (yellow) for three different energies (left, middle, right), each from two carbonate perspectives top (above) and side (below). The absorbing carbon atom is shown in brown, nearest neighbor oxygen atoms in red, and the second-nearest neighboring lithium atoms in green. Left, 290.35 eV and polarization perpendicular to the carbonate plane, the exciton is strongly p_z-like on the carbon and nearest oxygen atoms. Middle, 298.28 eV and polarization in the carbonate plane, the exciton is still localized p-like on the central carbon with some intensity on the neighboring oxygen atoms. Right, 300.53 eV and polarization in the plane, the exciton is largely similar to the middle-energy case but less localized. The visualization was created using VESTA.[44]